Obrabotka metallov (tekhnologiya, oborudovanie, instrumenty) = Metal Working and Material Science. 2026 vol. 28 no. 3 pp. 286–314
ISSN: 1994-6309 (print) / 2541-819X (online)
DOI: 10.17212/1994-6309-2026-28.3-286-314

NSTU NETI

Obrabotka metallov - Metal Working and Material Science

Journal homepage: http://journals.nstu.ru/obrabotka_metallov

Evaluation of the possibility of reducing residual austenite during laser carburization of low-carbon steel by additional cryogenic treatment

Antonina Karlina [1, a, *], ***Vitaly Gladkikh*** [1, b], ***Galina Vitkina*** [2, c], ***Roman Kononenko*** [2, 3, d], ***Viktor Kondratiev*** [2, 4, e]

[1] National Research Moscow State University of Civil Engineering, 26 Yaroslavskoe Shosse, Moscow, 129337, Russian Federation
[2] Cherepovets State University, 5 Lunacharsky pr., Cherepovets, 162600, Russian Federation
[3] Irkutsk National Research Technical University, 83 Lermontova str., Irkutsk, 664074, Russian Federation
[4] A.P. Vinogradov Institute of Geochemistry SB RAS, 1A Favorskiy St., Irkutsk, 664033, Russian Federation

[a] https://orcid.org/0000-0003-3287-3298, karlinat@mail.com; [b] https://orcid.org/0000-0003-1953-1584, gladkich_87@mail.ru;
[c] https://orcid.org/0000-0002-1076-2709, 20procents@mail.ru; [d] https://orcid.org/0009-0001-5900-065X, istu_politeh@mail.ru;
[e] https://orcid.org/0000-0002-7437-2291, imz@mail.ru

ARTICLE INFO

Article history:
Received: 08 June 2026
Revised: 16 July 2026
Accepted: 29 July 2026
Available online: 15 September 2026

Keywords:
Carburizing
Paste
Martensite
Ledeburite
Austenite

ABSTRACT

Introduction. Residual austenite is an austenitic phase that persists in steel after its incomplete transformation into martensite/bainite/ferrite. The presence of residual austenite in steel can cause positive or negative changes depending on its proportion. Therefore, the finished products must have an appropriate range of residual austenite content. In the process of traditional chemical and thermal treatment of metals by carburizing, residual austenite is an unacceptable defect in the process. Very few papers have been devoted to this issue in the processes of surface treatment of metals with concentrated energy sources. ***The purpose of this work*** is to reduce the residual austenite in the carburized layer after laser hardening using additional cryogenic treatment. **Materials and methods.** Laser carburizing of 0.2% *C* steel was performed with a continuous-wave ytterbium fiber laser (*LS-16*, 1.5 kW, *IPG Photonics*, Oxford, MA, USA) emitting at a wavelength of 1.07 μm. The carbon content in the carburized layer was determined by glow discharge optical emission spectrometry (*GD-Profiler 2*^{TM}). Hardness was measured using a semi-automatic *Vickers* hardness tester with a load of 500 g and an indentation pitch of 0.25 mm. X-ray diffraction patterns were recorded using a *SmartLab 9KW* diffractometer with a *Cu–Kα* target (**λ** = 1.5406 Å). The scanning angle range of 2θ ranged from 40 to 100°, and the scanning speed was 2°/min. Quantitative analysis of the volume fraction of residual austenite was carried out in accordance with the recommendations specified in *ASTM E975-13*. Cryogenic treatment was carried out at a temperature of –196 °C. **Results and discussion.** Different graphite contents in the laser carburizing pastes lead to the formation of different structures and phases (cementite, ledeburite, martensite, residual austenite) in the surface layer. Microstructural examination of the surface layer showed that the structure of the original material (0.2% *C* steel) consists of soft and ductile ferrite with hard pearlite. The thermal gradient on the surface of the molten carbon-containing mixture, created by the laser beam, transformed the original microstructure into martensite by dissolving the carbonaceous mixture and solidifying the austenitic phase into martensite through rapid cooling. At the same time, residual austenite is formed in the surface layer due to rapid cooling. It was shown that laser carburizing leads to the formation of a modified surface layer consisting of carbon-saturated martensite, residual austenite and carbides. Cryogenic and tempering treatments additionally transform residual austenite in the carburized layer into martensite, which increases the hardness of the carburized layer.

For citation: Karlina A.I., Gladkikh V.A., Vitkina G.Y., Kononenko R.V., Kondratiev V.V. Evaluation of the possibility of reducing residual austenite during laser carburization of low-carbon steel by additional cryogenic treatment. *Obrabotka metallov (tekhnologiya, oborudovanie, instrumenty) = Metal Working and Material Science*, 2026, vol. 28, no. 3, pp. 286–314. DOI: 10.17212/1994-6309-2026-28.3-286-314. (In Russian).

*** Corresponding author**
Karlina Antonina I., Ph.D. (Engineering), Research Associate
National Research Moscow State Construction University,
26 Yaroslavskoe shosse,
129337, Moscow, Russian Federation
Tel: +7 950 120-19-50, **e-mail:** karlinat@mail.ru

Introduction

Low-carbon steels are widely used in many industries due to their moderate tensile strength, affordability, good machinability, impact toughness, and ductility. However, their relatively low surface hardness and wear resistance limit their performance in challenging conditions [1, 2]. To address these issues and to expand the functionality of low-carbon steel machine parts, researchers have turned to surface modification techniques to improve their mechanical properties [1–10]. One of the most effective surface modification techniques is heat treatment, which involves the process of carburizing the surface layer of low-carbon steels. Carburization, a widely used thermochemical process, introduces diffusible elements such as carbon into the surface layer of steel at elevated temperatures, followed by quenching and tempering to increase hardness and wear resistance [1–3]. Machining operations on low-carbon steels intended for case-hardening are typically performed prior to the case-hardening process. At this stage, the low-carbon steel core remains relatively soft and ductile, allowing for efficient cutting, planing, and drilling with minimal tool wear [3–5]. Low-carbon steel exhibits superior machinability compared to carbon and alloy steels, primarily due to its high content of ferrite, the softest phase of steel. Hardening low-carbon steel through the process of case-hardening significantly improves its performance in many engineering applications where surface strength is critical.

Traditional carburizing methods – in solid, liquid, and gaseous media – are limited by long processing times, unstable atmospheres, intergranular oxidation, and dimensional distortion, especially in complex or thin parts [1, 2]. While low-temperature (vacuum) carburizing addresses many of these issues by offering faster carburization cycles, minimal oxidation, improved uniformity, and reduced distortion, it also has its drawbacks, including high initial investment, reliance on precise gas dosage and flow control, and the difficulty of adding hydrocarbons such as acetylene without forming soot or resinous deposits, limiting its widespread adoption [1–4]. Furthermore, traditional processes produce hazardous byproducts, generate CO_2 emissions, and pose problems with the disposal of spent carburizing compounds, making them environmentally unsustainable [5, 6]. Moreover, for many engineering applications, there is a trade-off between surface layer depth and core ductility, as excessive or deep carburized surface layer formation in thin parts can reduce overall tensile strength through thermal grain growth and increased residual stress. Therefore, surface hardness and core toughness must be carefully balanced during design.

An effective solution to the problem of reducing carburization time is surface saturation using concentrated heat sources. There are many methods of surface hardening with highly wear-resistant materials. These include, first and foremost, laser [8–12], electron beam [13–17], plasma [18–26], and electric arc [27, 28] processing.

Surface layers containing approximately 1.57–2.55 wt.% carbon were obtained by atmospheric electron beam surfacing of low-carbon steel plates with a mixture of iron and graphite powders [13–17]. The main process parameter determining the thickness, structure, and mechanical properties of the hardened layer was the electron beam current. With an increase in beam current from 20 to 26 mA, the thickness of the deposited layers increased from 1.2 to 2.6 mm, and the hardness decreased from 5.7 to 4.5 GPa. In friction tests with stationary abrasive particles, the wear resistance of the deposited layers was close to that of samples subjected to carburization in a powder environment. Laser carburization [8–12], as well as plasma carburization [18–28], is carried out mainly by melting the surface layer, onto which a carbon-containing powder mixture has been pre-applied. Laser surface alloying has been carried out experimentally for various substrates and alloying elements [8–10, 29–34]. Most of the published works [8–12, 29–34] concerning laser carburizing of steels have been carried out using this mechanism.

Hypereutectic carbon compositions have also been obtained in studies using an electron beam [13–17] and a plasma arc [18–28]. However, substrate recrystallization leads to crack formation, which is a significant drawback of the process and is explained by the inherently brittle nature of the resulting microstructures, which is facilitated by extremely high cooling and solidification rates. Another disadvantage of the process is the formation of gas porosity in the solidified surface layers.

It is known that martensite can be divided into high-carbon plate martensite and low-carbon lath martensite depending on the carbon content [2, 3]. Increased carbon content near the surface during

carburization to produce hypereutectic compositions (>4.3 wt.% *C*) of carburized layers [13–17, 22–29] promotes the formation of coarse-grained plate martensite and a significant amount of residual austenite, which consequently reduces the surface strength and negatively affects the overall characteristics of the material [1–3]. To reduce the content of residual austenite and increase surface strength, multi-stage heat treatment strategies are used, including double high-temperature tempering, secondary hardening, cryogenic treatment, and tempering at sub-zero temperatures.

In contrast to the melting mechanism, a possible laser carburizing mechanism involving substrate austenitization and subsequent solid-state diffusion of carbon into austenite has been very little studied [7–9, 29–33]. This mechanism is certainly closer to traditional gas and powder carburizing methods, but an important question arises regarding the possibility of producing solid-state carburized layers using laser radiation without surface melting. This is mainly due to the extremely high heating rates encountered during laser irradiation of steels, which are on the order of 10^4 K/s or even higher [7–10]. Furthermore, the time spent above the critical austenitizing temperature (soak time) is very short, which limits the time available for carbon diffusion into austenite. A better solution may be a direct laser hardening process in a controlled atmosphere. In a suitable gas environment, the laser beam is capable of inducing a chemical reaction near the steel surface, which makes it possible to modify its surface properties [29–33]. Thus, it combines the advantages of both gas carburizing and the laser beam, and eliminates the need for expensive furnaces and their control. Furthermore, a controlled atmosphere also ensures process uniformity and controllability. It is necessary to note the advantages of carburizing through a paste or coating [13, 14, 19–27] applied to the metal surface due to the simplicity of the application method, control of the carbon content in the paste composition, and the ability to localize carburization sites at a specific location on parts and tools. At the same time, the features of laser carburizing in both the gas and solid phases, with or without melting of the surface layer at high heating rates, which are on the order of 10^4 K/s or even higher [8–10], contribute to the incompleteness of the martensitic process during the cooling stage, which leads to the formation of residual austenite (*RA*) in the hardened layer. Our analysis of open sources of information shows that the issue of residual austenite has not received sufficient attention from scientific schools of laser [8–12], electron beam [13–17], and plasma [19–28] surface carburizing. At the same time, extensive theoretical and experimental research has been accumulated in the field of traditional furnace thermochemical methods for processing various metals [1–5, 34–44].

It is known [1, 2, 36, 41, 42] that residual austenite is found in steels when austenite is not completely transformed into product phases. The term “residual austenite” refers to austenite that does not undergo transformation at room temperature. The stability and amount of residual austenite are important factors in steel design. Although studies have shown that residual austenite improves the mechanical properties of steel, its tendency to transform into martensite upon further undercooling or applied stress can also be undesirable. For example, while residual austenite has been reported to improve the service life of bearings under rolling fatigue, its excessive amount can degrade the dimensional stability of bearings [37–40]. The presence of residual austenite in steel can cause positive or negative changes depending on its proportion. Therefore, an appropriate range of residual austenite content is desirable in finished products such as gears, bearings, and tools. To improve the life of bearings in various applications, their microstructure must be appropriately tuned for their intended use. For example, bearings in gearboxes can fail prematurely due to cracking in the bearing steel if the required *RA* content is not maintained [37–40]. Increasing the *RA* content (> 20%) in these bearings has been reported to provide relatively long service life in such applications.

The influence of carbon saturation duration on the amount of residual austenite in medium-carbon steels *0.4% C–1% Cr*, *0.35% C–1% Cr–1% Mn–1% Si*, and *42CrMoS4* was examined in [4–6]. Increasing the saturation time from 8 to 12 hours resulted in an increase in residual austenite from 7% to 14%.

The authors of [41] demonstrated that direct assessment of the amount of austenite remaining unchanged after full quenching using X-ray diffraction analysis is difficult because the high-intensity peaks of austenite and martensite overlap and merge, and austenite transforms into martensite during sample preparation due to its low stability. The results indicate that the amount of residual austenite in a fully quenched low-carbon steel sample is underestimated using standard X-ray diffraction spectroscopy.

However, according to the authors of [41], even this small amount of residual austenite can be detected after a short heat treatment (heating to temperatures of 200–400 °C), which leads to enrichment of the austenite with carbon. Due to the depletion of martensite in carbon and the accompanying enrichment of austenite, the peaks are separated and resolved.

In [42], a magnetoinductive method for assessing various levels of residual austenite content in case-hardened *20NiCrMo7* bearing steel is investigated, and a comparison is made with corresponding measurements by X-ray diffractometry and image analysis using an optical microscope. The residual austenite content in case-hardened *20NiCrMo7* steel was modified by additional tempering; the magnetoinductive method provides accurate results (with an average deviation of 0.5%) with sufficient sensitivity at various levels (including values below 5 vol.%) of residual austenite.

In [45], photographs of microstructures and carbon content are used to train machine learning models for predicting the residual austenite of case-hardened steel. To establish the relationship between chemical elements, microstructure, and mechanical properties, it is first necessary to accurately determine the microstructure metallographically. The neural network establishes a mapping from the feature space to the target attribute without considering any complex internal transformation laws; instead, it converts the process into a set of trainable weights that can theoretically approximate any type of nonlinear transformation. Thus, it is crucial to be able to accurately segment photographs of steel microstructures [45]. Results show that the accuracy of segmentation based on microstructure photographs using the model reaches 95.2%.

Cryogenic treatment (*CT*) is widely known for its effectiveness in reducing the proportion of residual austenite and stabilizing phases at room temperature [46]. During *CT*, the material is held at a temperature well below the martensitic transformation completion temperature (*Mf*) for a certain time, followed by a reheating process to room temperature [1–10, 42–44].

In [47], a comprehensive technological process for steel was developed that included carburizing, tempering, quenching, and cryogenic treatment. The carburized samples were characterized by analyzing the carbon profile, residual austenite content on the surface, microstructure, and hardness profile. Steels *17Cr2Ni2MoVNb* and *20Cr2Ni4A* had a similar microstructure after carburizing, consisting of high-carbon acicular martensite, carbides, and residual austenite in the surface layer and low-carbon lath martensite in the core. The depth of the carburized layer was approximately 1.4 (±0.05) mm. A good microstructure with acicular tempered martensite, less residual austenite, fine-grained dispersed carbides, and no oxides was obtained. The hardness of the samples near the surface after cryogenic treatment increased by 102–122 HV.

We have previously indicated that ledeburite structures are formed in the carburized layer during surface carburization [13, 14, 24]. Of interest is the work [48], where the microstructure of *Vanadis 6* ledeburite steel was investigated after treatment at sub-zero temperatures of –140 °C for different periods of time, followed by different tempering modes. The results obtained allow the authors to draw the following conclusions:

(1) the amount of residual austenite decreases fivefold as a result of this treatment, and compressive stresses above 1,500 MPa arise in this phase;

(2) during treatment at sub-zero temperatures of –140 °C, a large number of "additional" cementite carbides are formed; this amount is higher than that achieved during treatment at sub-zero temperatures of –196 °C.

A review of the literature on both traditional carburizing methods and those using concentrated heat sources shows that the carburizing process is a critical technology for improving the surface characteristics and mechanical reliability of metals. However, it is associated with a number of problems and limitations that can impact its effectiveness. Reducing residual austenite in traditional carburizing methods is a particular focus. Cryogenic treatment is currently the only operation capable of reducing its content in carburized steel [47–49].

Recent research findings highlight both the advances and critical challenges associated with carburizing methods [29–33]. Precise control of carbon potential, temperature, and holding time is necessary to achieve uniform hardening depth and carbon concentration, but deviations can result in residual austenite, brittle carbide networks, or incomplete hardening due to insufficient carbon diffusion [1–10].

In [33], a literature review was conducted in the field of laser surface heat treatment of steels. The authors showed that between 2008 and 2024, the number of publications devoted to laser processing of steel

increased almost 20-fold. By 2024, the number of articles remained at a level of over 200. This demonstrates significant interest in the technology of laser surface hardening of both plain steels and case-hardened steels in various centers around the world and confirms the statement that it has significant application potential with measurable economic benefits. At the same time, we note that in this review [33], priority was given to publications containing detailed numerical and descriptive data related to the laser processing (hardening) process, such as laser power, scan speed, spot diameter, type of laser source, final hardness, and chemical composition of steel. Initially, this was a database containing about 100 of the most relevant studies. The review does not contain any references to a separate area of laser application in chemical-thermal processing processes, except for the two works [29–32] that we cited above.

This paper presents a laser hardening method using a graphite mixture applied to the surface of low-carbon steel, which was remelted with the surface metal layer using laser radiation, followed by additional cryogenic treatment.

The purpose of the study is to reduce the residual austenite in the case-hardened layer after laser hardening using additional cryogenic treatment.

To achieve this purpose, ***the following tasks*** must be completed:

– to study the microstructure and microhardness distribution of the surface layer of low-carbon steel after laser reflow carburizing;

– to study the effect of cryogenic treatment on the hardness and residual austenite content of the hardened layer.

Materials and research methods

As a basis for obtaining a carburized surface layer, *0.2% C* steel was used – a low-carbon, high-quality structural steel known for its high strength, good machinability, weldability, and malleability. The typical chemical composition of *0.2% C* steel according to *GOST 1050-2013* is: 0.17–0.24% *C*, 0.35–0.65% *Mn*, 0.17–0.37% *Si*, ≤0.030% *P*, ≤0.030% *S*. It has a minimum tensile strength of 450 MPa and a yield strength of 245 MPa. Elongation to failure can reach 35–40%. It is readily cold- and hot-drawn using appropriate forming equipment. The dimensions of the samples for laser processing were 100×40×10 mm. A graphite-containing mixture (*EGS*-grade graphite) was applied to the surface of the *0.2% C* steel sample.

Fig. 1 shows the graphite fragments used in the powder composition. The detailed technology for applying the graphite mixture in the form of a paste-like mass to the surface of the samples is described in detail in the authors' previous works [13–29]. Laser modification of the surface with the deposited graphite layer was carried out using a processing unit equipped with a continuous-wave ytterbium fiber laser (*LS-16*, 1.5 kW, *IPG Photonics*, Oxford, MA, USA), emitting at a wavelength of 1.07 μm. Table 1 shows the modes in which the laser saturation process was carried out.

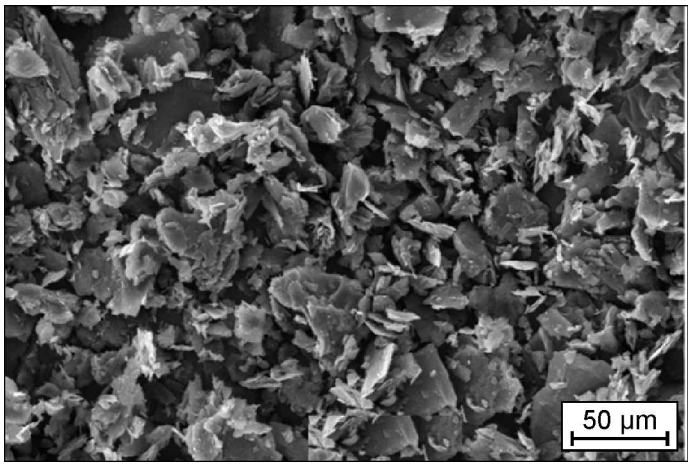

Fig 1. Fragments of graphite coating particles with a size of < 0.08 mm

Table 1

Parameters of the saturation process

Distance to sample surface (mm)	Traverse speed (mm/s)	Laser power (kW)	Graphite content (%)	Coating specific weight (g/m^2)
5	3	1.0	10	100–120
5	3	1.0	25	130–150
5	3	1.0	50	160–180
4	10	1.5	10	80–100
4	10	1.5	25	110–130
4	10	1.5	50	140–160

The carbon content of the carburized layer was determined using glow discharge optical emission spectrometry (*GD-Profiler 2*^{TM}). Hardness was measured using a semiautomatic *Vickers* hardness tester (*MH-500*) with a load of 500 g and an indentation step of 0.25 mm. X-ray diffraction spectra were recorded using a *SmartLab* 9KW instrument with a *Cu-K*$\boldsymbol{\alpha}$ target and an X-ray wavelength ($\boldsymbol{\lambda}$) of 1.5406 Å. The scanning angle range 2$\boldsymbol{\theta}$ was from 40 to 100°, and the scanning speed was 2°/min. Quantitative analysis of the volume fraction of residual austenite was carried out in accordance with the recommendations specified in *ASTM E975-13* [49]. The volume fraction calculation was based on the integrated intensities of the diffraction peaks (200)$\boldsymbol{\gamma}$, (220)$\boldsymbol{\gamma}$, (311)$\boldsymbol{\gamma}$, (200)$\boldsymbol{\alpha}$, and (211)$\boldsymbol{\alpha}$. In addition, the average carbon concentration in the residual austenite ($C\boldsymbol{\gamma}$, in wt.%) was determined using equation (1) [46, 47]:

$$C_{\gamma} = \frac{(\alpha_{\gamma} - 3.547)}{0.046}, \quad (1)$$

where $\boldsymbol{\alpha}_{\gamma}$ is the lattice parameters of residual austenite (in Å), determined from the positions of the (200)γ and (220)γ diffraction peaks.

Microstructural studies were conducted using scanning electron microscopy (*Zeiss Auriga Compact SEM*). The surface layer microstructure was examined using a *MET-2* optical microscope. Residual austenite content was measured using *Stream Essentials Olympus* image analysis software.

To evaluate cryogenic treatment, the laser-carburized samples were immersed in liquid nitrogen at –196 °C for 2, 5, and 10 hours. Additionally, to study the effect of cryogenic treatment duration, the samples were tempered at 200 °C for 2 hours. The experimental setup is shown in Fig. 2.

Research results

The surface appearance of the specimens after laser carburizing is shown in Fig. 3. Fig. 3,*a* shows the surface appearance before paste application. Fig. 3,*b*, *c* shows the surface after laser treatment with different

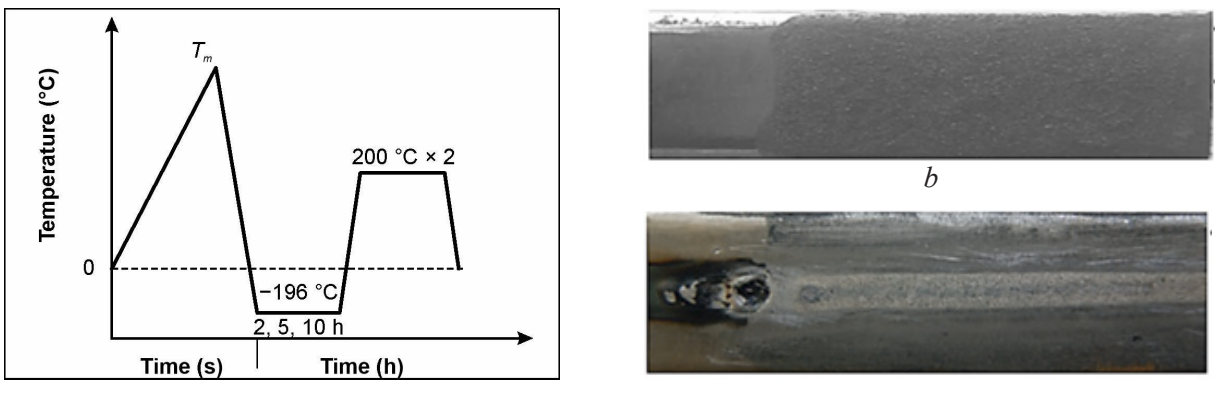

a *b* *c*

Fig. 2. Laser saturation process with different durations of cryogenic treatment and tempering (*a*); sample with graphite paste (*b*); sample after laser melting of graphite paste (*c*)

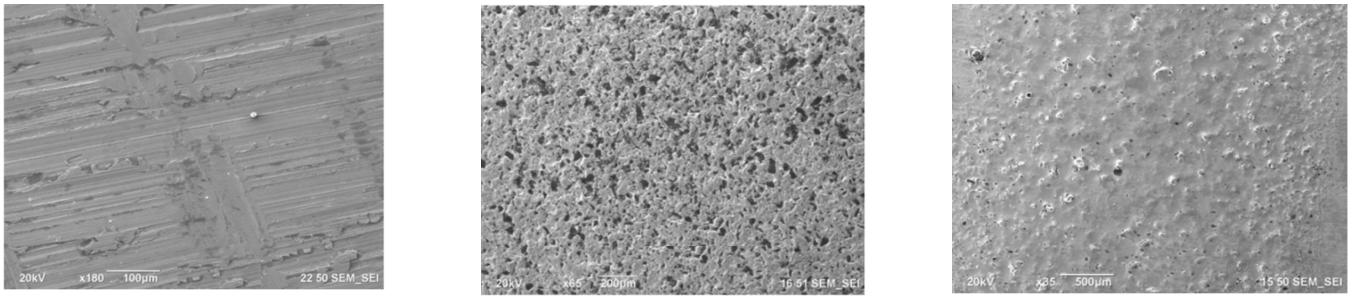

a *b* *c*

Fig. 3. Surfaces of samples after laser carburizing:
a – original surface; *b* – after application of powder mixture (25% graphite); *c* – 50% graphite

laser powers. It can be seen that at a power of 1 kW, graphite particles remain on the melt surface. With an increase in power to 1.5 kW, the surface has a minimal number of unmelted particles.

Fig. 4,*a* shows a cross-section after applying a coating with 10% graphite. Fig. 4,*b* shows a cross-section after applying a coating with 25% graphite. Fig. 4,*c* is a volumetric photograph taken using an electron microscope, which simultaneously shows the coating surface and a cross-section along the depth. It is evident that the depth of the carburized layer is no more than 100 µm (Fig. 4). Next comes the heat-affected zone with structures characteristic of surface hardening. The carburized layer in Fig. 4,*a*, *b* is beneath the surface, distinguished by its dark yellow color. This layer is uniform and extends to a depth of 50 ± 0.1 µm. A white layer – residual austenite – is clearly visible. Optical micrographs in Fig. 4,*a*, *b* reveal the presence of residual austenite (light areas) with lath and plate martensite (dark areas). This process is well described in the literature on this topic. Two types of residual austenite – blocky and film morphology – were detected in the samples.

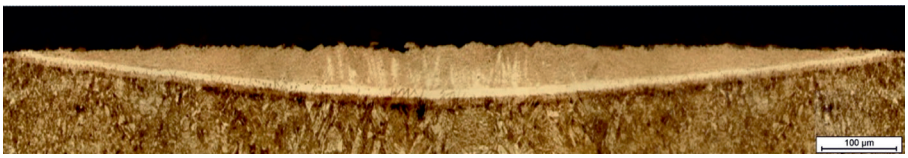

a

b

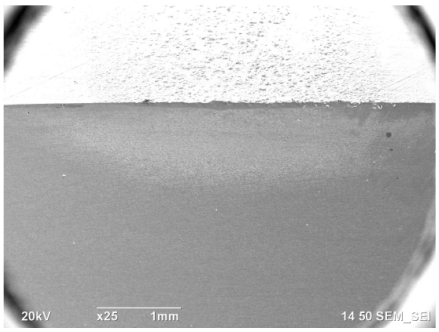

c

Fig. 4. Hardened layer in the metal after melting of the powder mixture in cross section:
a – optical metallography, 10% graphite; *b* – optical metallography, 25% graphite; *c* – *SEM* image, 10% graphite

Experiments revealed that increasing the graphite content in the powder mixture to 50% yielded eutectoid and hypereutectic carbon compositions with high levels of residual austenite (Fig. 5). The gradient distribution of microhardness values (Fig. 6) is a good indicator of carbon content (distribution) across the layer cross-section. Residual austenite is readily discernible on transverse metallographic sections of the carburized layer under optical microscopy (Figs. 4, 5, 7, 8). The carbon content across the depth of the carburized layer was determined for each powder mixture composition; the results are summarized in Table 2.

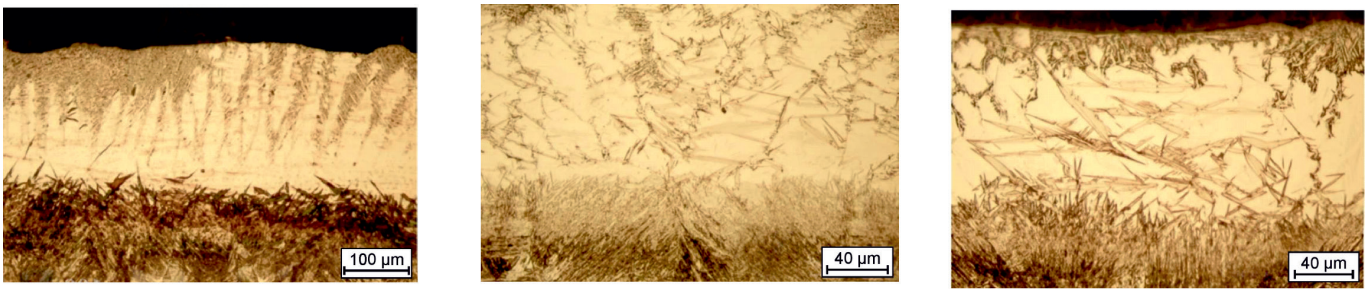

a *b* *c*

Fig. 5. Hardened layer in the metal after melting of the powder mixture in cross section:
a, *b* – optical metallography, 25% graphite; *c* – optical metallography, 50% graphite

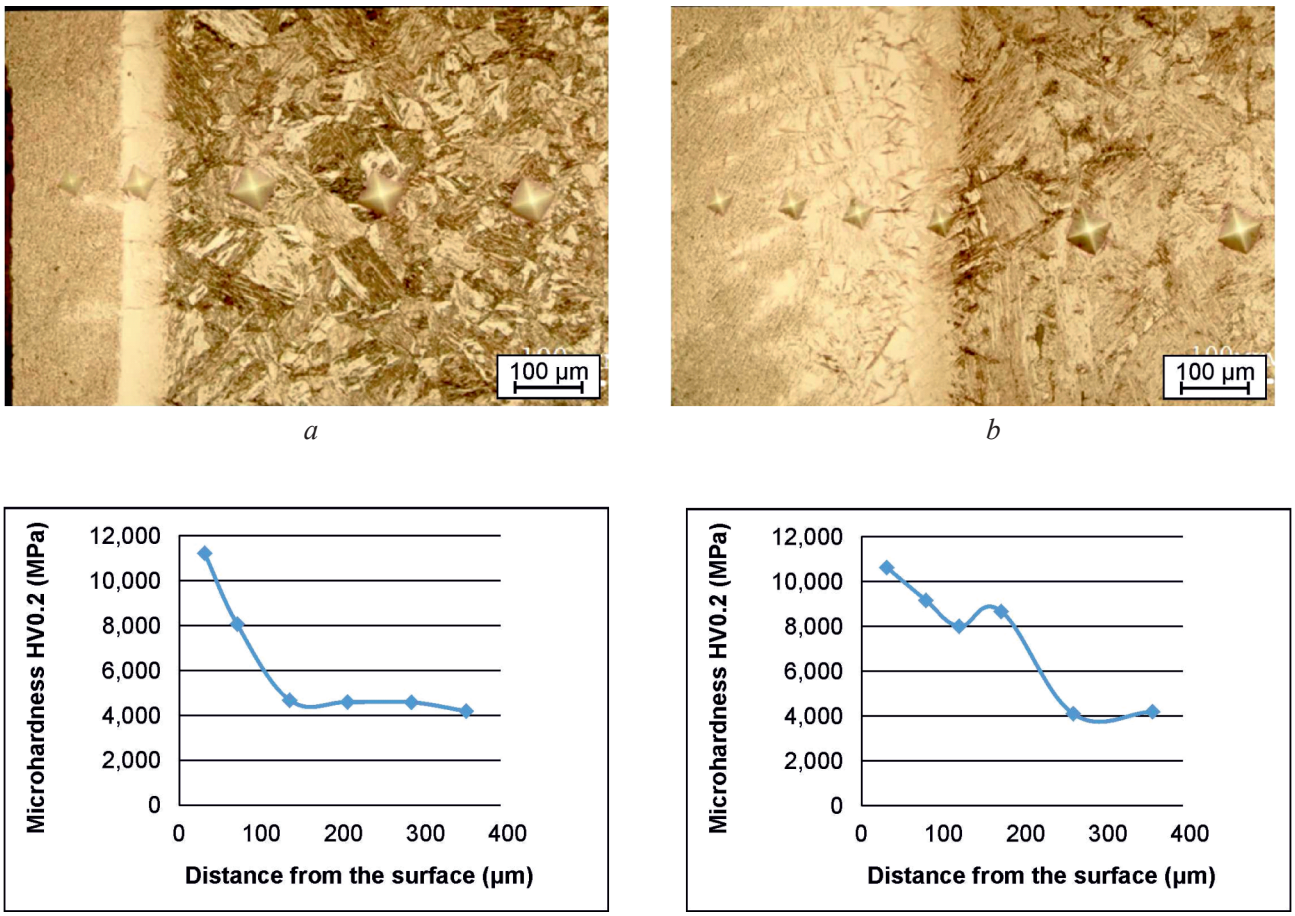

a *b*

c *d*

Fig. 6. Surface layer after laser carburizing by depth:
a – 50% graphite; *b* – 25% graphite; *c* – microhardness distribution, 50% graphite; *d* – microhardness distribution, 25% graphite

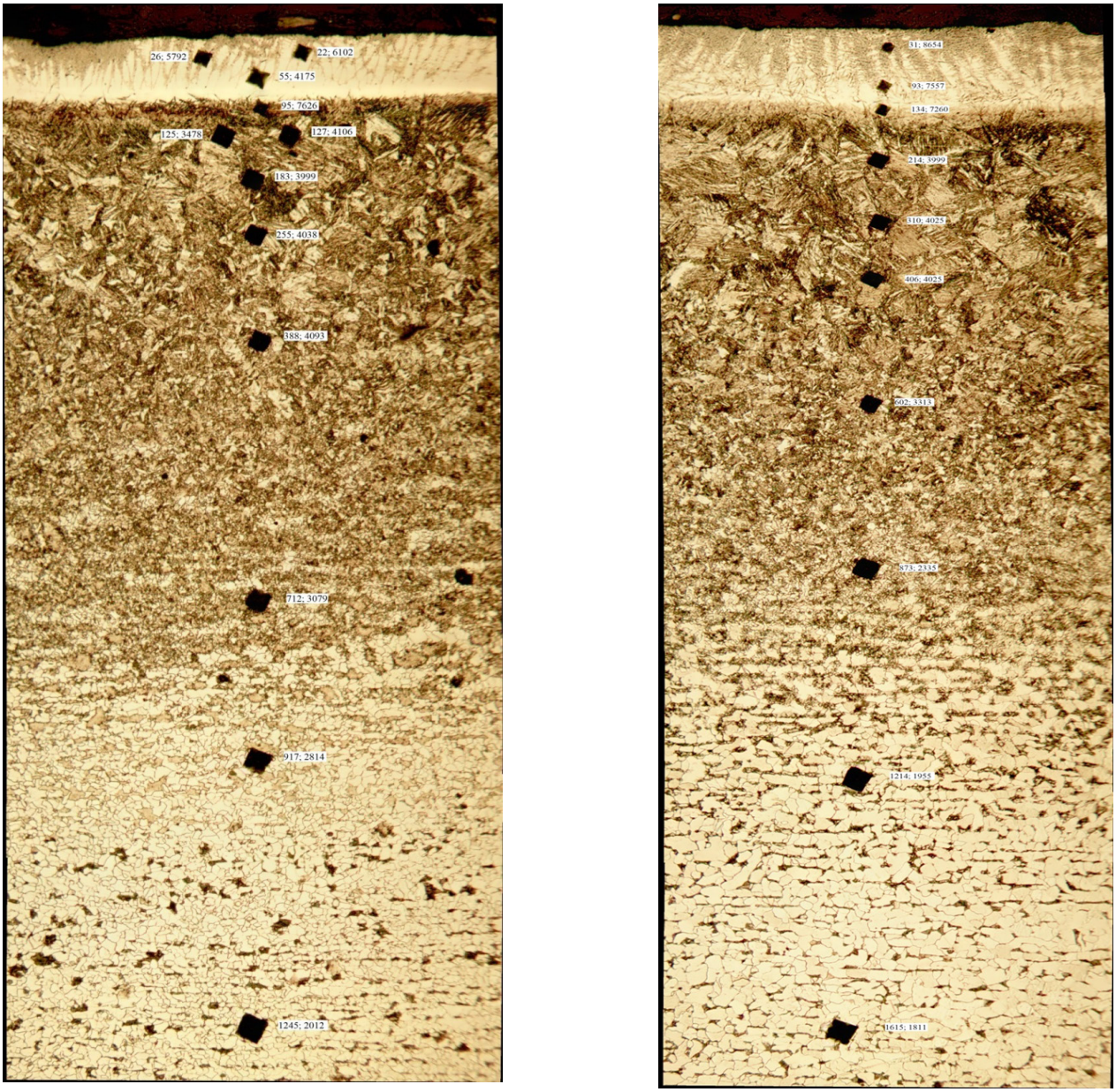

a *b*

Fig. 7. Panoramic image of the surface layer depth after laser carburizing with microhardness distribution by layers (carburized layer, heat-affected zone, transition layer to the base metal):
a – 25% graphite; *б* – 50% graphite

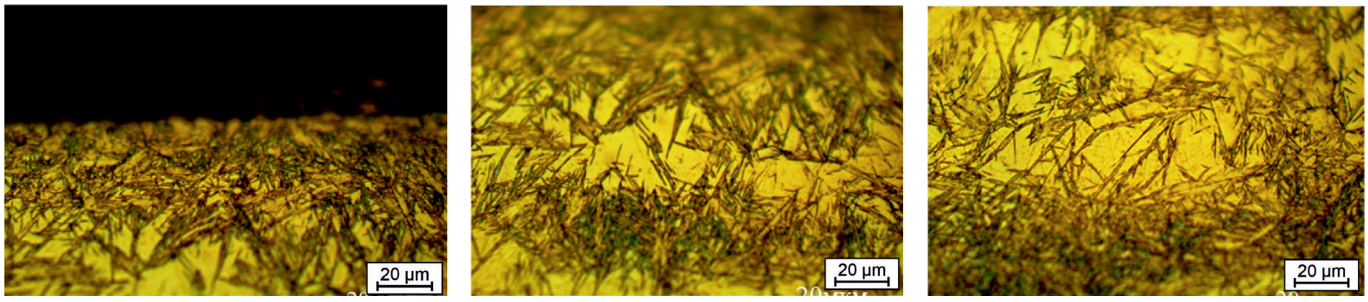

a *b* *c*

Fig. 8. Optical metallography of layer fragments by depth after processing with a powder mixture containing 10% graphite:
a – at the surface; *б* – middle of the layer; *в* – transition to the base metal

Table 2

The carbon content in the surface layer of *0.2% C* after laser carburizing from the paste composition

Depth (μm)	*C* content (10% graphite coating)	*C* content (50% graphite coating)
0	0.8	2.4
200	0.6	1.8
500	0.4	1.2

Using X-ray diffraction analysis, shown in Fig. 9, the volume fraction of residual austenite was determined. It was found that the original surface of *0.2% C* steel was free of residual austenite at room temperature (Fig. 9,*a*). After laser surface carburizing with a 50% graphite coating, austenite peaks were detected (Fig. 9,*b*). To further quantify the fraction of residual austenite in the specimens machined at 3 mm/s and 1 kW laser power with 50% graphite content, the X-ray diffraction profiles corresponding to the carburization depths of 20, 60, 120, 190, 280, and 500 μm were ground after machining and analyzed, as shown in Table 3. All the obtained diffraction patterns had the same peak distribution along the carburized layer depth (as in Fig. 9b) and differed only in the peak width and height. The peaks of quenched martensite and residual austenite were found. The diffraction peaks for γ, namely (200), (220), and (311), as well as the peaks for α (200) and (211), were analyzed. At depths from 60 to 280 μm, the maximum amount of residual austenite was recorded in the range from 11 to 21%.

The laser-carburized surface layer areas examined by X-ray diffraction were simultaneously studied using optical microscopy (Table 4). Evaluation was based on grayscale images to obtain the percentage of residual austenite per unit area. Assuming a random grain distribution and isotropic grain growth, the

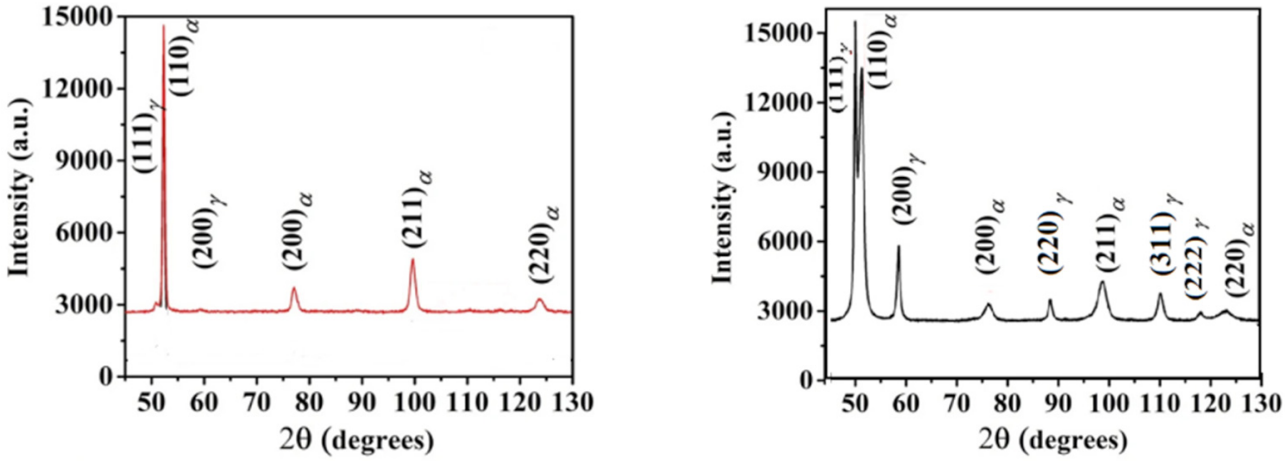

a *b*

Fig. 9. X-ray diffraction patterns:
a – initial 0.2% *C* steel; *b* – after laser carburizing with 50% graphite paste

Table 3

Distribution of martensite and residual austenite according to X-ray diffraction analysis after laser carburizing with 50% graphite coating

Depth (μm)	Martensite (%)	Austenite (%)
20	95.99631845	4.003681549
60	78.00152027	21.99847973
120	83.2360707	16.7639293
190	82.97027584	17.02972416
280	88.87531497	11.12468503
500	95.60167217	4.398327833
580	99.50605689	0.493943112

Table 4

Results of residual austenite measurements at different depths by optical metallography

Sample	Depth (μm)			
	0	0.1	0	0.5
10% graphite coating	2.1	10% graphite coating	2.1	10% graphite coating
25% graphite coating	6.2	25% graphite coating	6.2	25% graphite coating
50% graphite coating	12.3	50% graphite coating	12.3	50% graphite coating

percentage per unit area was taken to be equal to the volume percentage. Fig. 8,*a–c* which shows the representative microstructure of all samples, confirms the presence of martensite and residual austenite in each sample. In addition, Fig. 8 shows representative color images of the sample obtained using optical microscopy. The appearance of homogeneous martensite (dark) and residual austenite (white) in color facilitates the measurement of the proportions of individual phases.

Fig. 10 shows the results after cryogenic treatment and tempering. Fig. 10,*a* shows the initial residual austenite content after laser carburization with a composition of 20% graphite. Fig. 10,*b* shows the structure after 2 hours of holding at –196 °C. The optical images reveal a decrease in residual austenite; calculation using the software showed a reduction of up to 10%. Fig. 10,*c* corresponds to a holding time of 5 hours. To further quantify the proportion of residual austenite, X-ray diffraction profiles corresponding to the carburization depths were examined after cryogenic treatment and tempering, as shown in Table 5. Peaks of quenched martensite and residual austenite were identified.

The diffraction peaks for γ, namely (200), (220), and (311), as well as the peaks for α (200) and (211), were analyzed. The amount of residual austenite decreases across the entire depth.

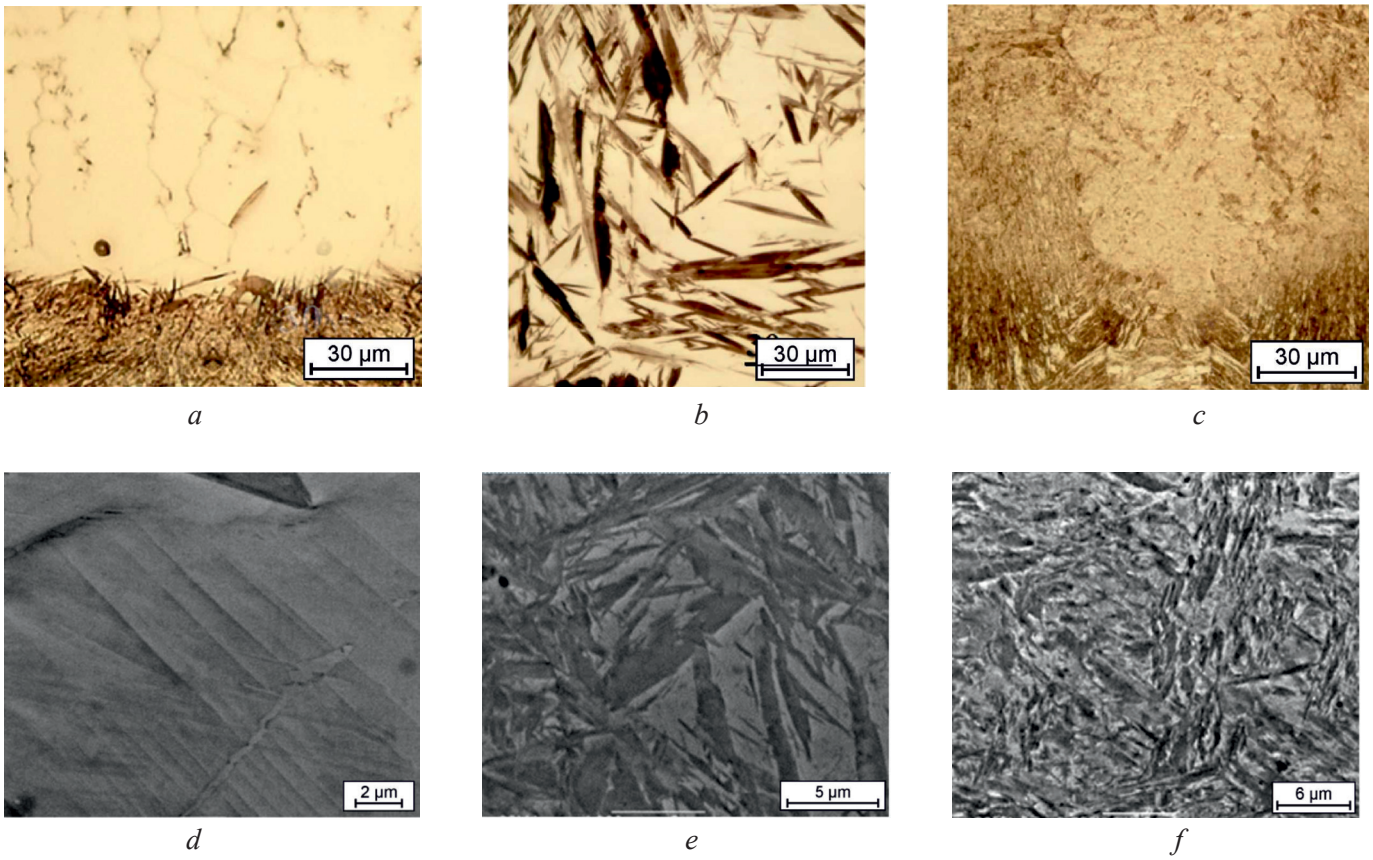

a *b* *c*

d *e* *f*

Fig. 10. Microstructure of the carburized layer after cryogenic treatment and tempering:

a, *d* – initial residual austenite content 20%; *b*, *e* – after 2 h of holding at –196 °C, decreased to 16%; *c*, *f* – holding for 5 h, decreased to 10%

Table 5

Distribution of martensite and residual austenite according to X-ray diffraction analysis after cryogenic treatment (5 h) and tempering

Depth (μm)	Martensite (%)	Austenite (%)
20	99.50605689	0.493943112
60	94.60167217	5.398327833
120	88.87531497	11.12468503
190	92.97027584	7.02972416
280	98.990674	1.009326002
500	99.50605689	0.493943112
580	99.44403915	0.555960854

Fig. 11 presents a combined compilation of the study results, showing the microstructure of martensite and residual austenite together with the distribution of microhardness values across the layer depth. A hardness dip is evident in the zone with the maximum amount of residual austenite. After cryogenic treatment for 2 hours and tempering, this dip in hardness is eliminated due to the transformation of residual austenite to martensite (Fig. 12). Cryogenic treatment for 10 hours did not have a positive effect on reducing residual austenite in the carburized layer. Note the increase in microhardness after cryogenic treatment (Fig. 11).

Results and discussion

Before discussing the obtained results, it is necessary to formulate the thesis that, during the course of our experiments, we obtained a supersaturated carbon metal in the surface layer of *0.2% C* steel, which, in terms of the phases and structures formed within it, has nothing in common with the base material. We used *0.2% C* steel solely as a substrate for surface carburizing. Naturally, when analyzing the phases and

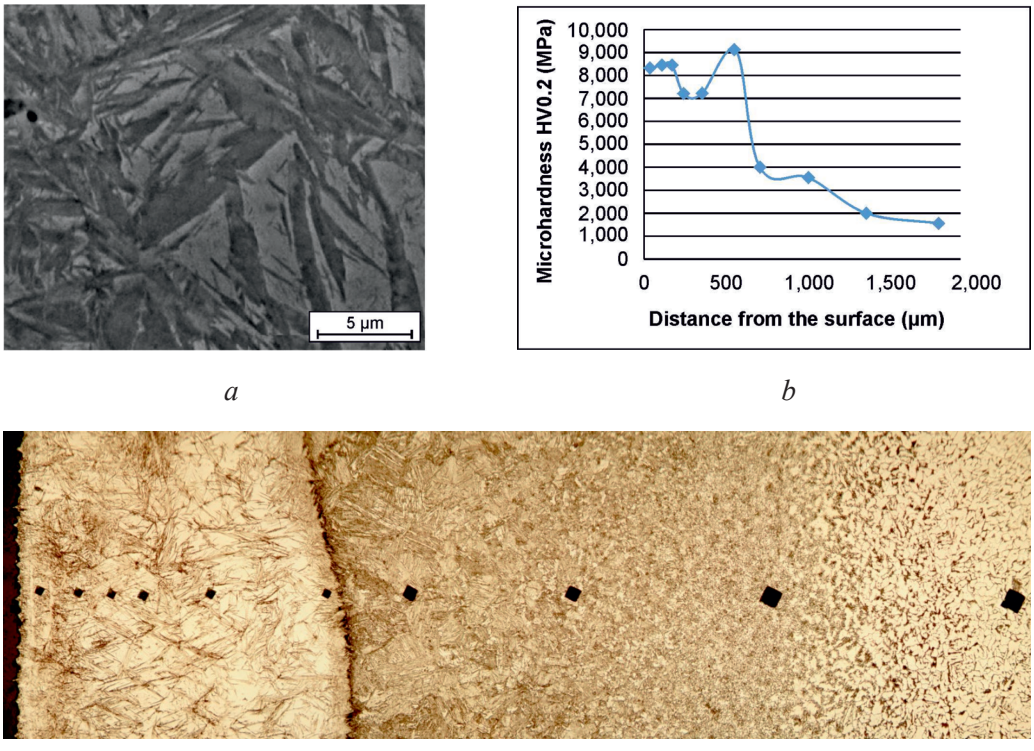

a *b*

c

Fig. 11. Summary of research results after laser carburizing in modes with surface melting at a speed of 3 mm/s (25% graphite):

a – microstructure of the layer (martensite); *b* – microhardness distribution by hardening depth; *c* – panoramic optical image of the hardened zone by depth

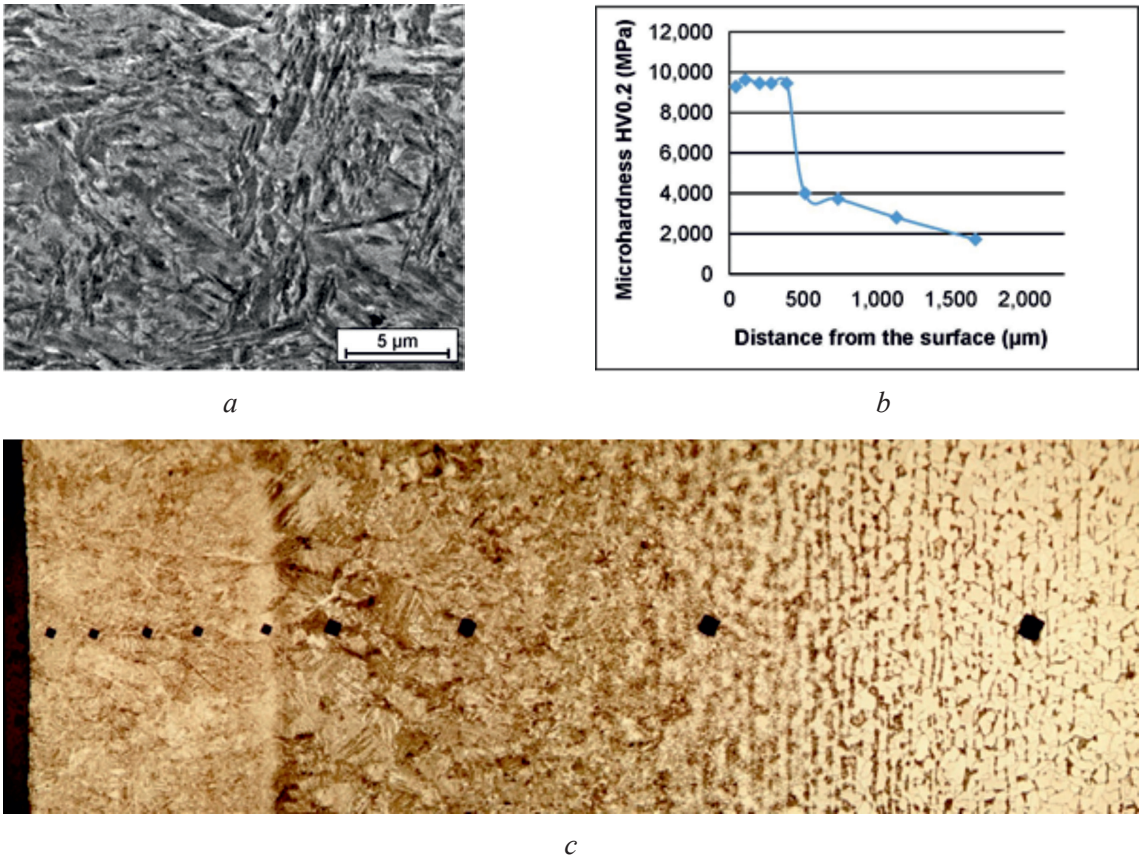

a *b*

c

Fig. 12. Summary of research results after laser carburizing in modes with surface melting at a speed of 3 mm/s (25% graphite) + cryogenic treatment and tempering:
a – microstructure of the layer (martensite); *b* – microhardness distribution by hardening depth; *c* – panoramic optical image of the hardened zone by depth

structures, we will refer to the works of other authors, where similar phase and structural transformations have been studied [13–29].

Fig. 4 shows optical microscope images of the samples, corresponding from left to right to the surface layer, subsurface layer, transition layer, and core. After laser surface carburizing, the surface layer consists mainly of cementite, while the subsurface layer consists of finer acicular martensite and residual austenite. The distribution of martensite and residual austenite based on X-ray diffraction analysis after laser carburizing is presented in Table 2. It is evident that the residual austenite content is distributed non-uniformly across the depth.

Further research is needed to more accurately understand the dependence of the residual austenite formation process on the laser carburizing conditions. Currently, we can confirm for the first time that this problem exists in the laser carburizing process, and it has not been previously addressed in studies [13–26]. The question of whether this is beneficial or detrimental remains open, as the primary goal of laser carburizing is to increase hardness and wear resistance.

Figs. 5–8 show optical microscope images of the samples, representing from left to right the surface layer, subsurface layer, transition layer, and core. Overall, the panoramic images show that laser carburizing results in the formation of a carbon-rich layer with a distinct fusion line with the base metal. However, the base metal along the fusion line was heated below the melting point, revealing a heat-affected zone (*HAZ*) within it, where quenched structures also formed. Thus, a unique composite layer was formed.

When the graphite content of the powder mixture is up to 25%, the surface layer consists mainly of acicular martensite and residual austenite, while the subsurface layer consists of finer acicular martensite and residual austenite. With decreasing carbon content, the microstructure of the transition layer is mainly represented by lath martensite and a small amount of acicular martensite, while the core consists mainly of

lath martensite due to the long holding time. A large amount of residual austenite is visually recorded during optical imaging (Figs. 4, 5) at a graphite content of 50% in the powder mixture, which coincides with the results of studies obtained using electron beam processing without vacuum [13–16] and plasma [21–29] during carburization of low-carbon steel plates with a mixture of iron and graphite powders.

The main structural components in the deposited layers [13, 14, 21, 22] were ledeburite, secondary *Widmanstätten* cementite, and pearlite. The formation mechanism of ledeburite, cementite, and pearlite at a content of up to 50% and more in the powder mixture is discussed in detail in [13, 14, 21–26]. To obtain a high-carbon martensitic structure, the authors of [13] recommend increasing the thickness and weight of the workpiece or decreasing the thickness of the hardening layer directly during the deposition process by increasing heat transfer into the colder volume of the workpiece.

Microstructural analysis of the surface carburized layer in case-hardened low-carbon steel also reveals significant changes in grain morphology and distribution in different zones. The microstructural gradient from surface to core emphasizes the diffusion-driven nature of case-hardening, resulting in a hardened outer layer with increased carbon content tapering to a softer, ductile core (Figs. 7, 11, 12). This microstructural profile is desirable because it combines surface wear resistance with core strength — an important property for structural applications requiring durability. Micrographs also confirm that higher graphite contents in the paste during carburizing treatment promote higher carbon saturation, which leads to improved mechanical properties, particularly hardness [13–23]. Optical metallography revealed a visible contrast between the surface layer and the core after etching, allowing for a qualitative assessment of the surface layer depth. These results confirm the effectiveness of carburizing in improving surface properties while maintaining core strength [2, 3], and are consistent with the results of other authors [13–26].

After cryogenic treatment (Figs. 10, 12) and tempering, some of the residual austenite undergoes further transformation, and the martensite content in the surface layer of the specimen further increases, while the transition layer and core primarily consist of tempered lath martensite.

Measurement of the residual austenite content at various depths using optical microscopy (Table 4) revealed a similar trend to that obtained by X-ray diffraction (*XRD*) measurements (Table 3). However, this method is difficult to accurately quantify at low levels of residual austenite (<2%) [34–39]. To address concerns about the quantitative discrepancy of nearly 1.5 times between the two methods used to determine residual austenite, we provide the following explanation.

It is important to note the main thesis of our work: our research did not aim to evaluate the accuracy of each method. We simply used two methods for comparison to identify the role and/or influence of cryogenic treatment on the transformation of residual austenite. For these purposes, we needed to use two methods specifically to understand how the process of surface saturation of steel with carbon occurs, what structures and phases are formed within it, and how cryogenic treatment influences these processes.

From the point of view of the accuracy and reliability of the residual austenite values obtained by the two methods, we note that the optical method refers to the qualitative assessment of residual austenite [2, 3], since despite clear visualization (see Figs. 5–8), a large study area (typical measurement area >100 μm^2), ease of sample preparation, and the equipment used (optical microscope) in the process of studying residual austenite, it has limitations in terms of determining film-type residual austenite (located along the boundaries of martensite plates) and, most importantly, there is a high probability of erroneous interpretation with iron carbide [50], which also has a white tint when viewed through an optical microscope [51]. To eliminate erroneous interpretation, it is necessary to additionally use a microhardness tester. The next point that is important to consider is how to select the appropriate etchant (usually 3–5% nitric acid in alcohol is used), since the etching time and intensity can greatly change the contrast of the structure so that untempered (tetragonal) martensite plates cannot be distinguished from residual austenite.

There is no specific regulatory document for the method of determining residual austenite in the Russian Federation. References exist to *GOST 8233–56 "Steel. Microstructure Standards"* and *GOST 11878–66 "Austenitic Steel. Methods for Determining the Ferrite Phase Content in Rods"*. The latter regulatory document states: *"On each section, at a magnification of 280–320 and a microscope field of view diameter of 0.38–0.43 mm, the location with the highest content of the phase under study is determined. This is*

visually assessed in points or as a percentage by comparison with photo standards on the attached scale". The regulatory document (Microstructure Standards) does not specify the austenite structure. Given the above, optical microscopy provides qualitative data with a subjective quantitative estimate; however, it is difficult to determine the residual austenite content below 5%. The author of [51] notes that optical microscopy yields a deviation of up to 20% depending on the residual austenite content and tempering. This method is subjective and yields wide variations in results. Therefore, some companies have developed their own corporate standard micrographs [51]. Given this, optical metallography data should be considered as qualitative indicators for assessing the formation of residual austenite in the surface layer during laser carburizing using pastes containing 10 to 50% graphite.

Measurement by X-ray diffraction (*XRD*) is recognized by most researchers as a reliable instrumental method for measuring residual austenite in steel (measurement error up to 0.1%) [34, 37, 39, 41, 46, 48, 49, 52]. However, the presence of carbides [50, 51] may influence the determination of residual austenite. This influence is due to the presence of overlapping or adjacent carbide peaks, which can interfere with and change the intensity of the ferrite or austenite peaks. The standard algorithm based on the assessment of the region of interest may lead to an incorrect estimate of residual austenite [51, 52], since it may be fully or partially taken into account when integrating the peaks. Using a full-profile approach, it is possible to account for the influence of this peak and ignore it, as well as any other carbide peaks that may interfere. At the same time, as the author notes [51], the presence of additional phases and reflections caused by grain size, carbides, or texture can cause distortions and deviations.

Many researchers believe that the *EBSD* method can provide a more accurate picture of the residual austenite in the carburized layer compared with the optical method and X-ray diffraction. However, this is not the case, and the *EBSD* method has even more limitations than the two methods presented above [53, 54]. The first is the size — very small sample dimensions (no more than 5 mm for a square side) and a sample thickness of no more than 1 mm. In addition, the survey itself is carried out on an even smaller area of the sample (a map of no more than 100 μm is constructed), i.e., this is a local, non-representative sample. And if we also take into account that in our case an uneven distribution of martensite and residual austenite (see Fig. 8) in the mapping area is possible, then this method does not give us anything in terms of quantitative values. The authors [53] note that it is possible to construct maps larger than 100 μm, but this increases the survey time to 24–120 hours.

The second requirement is surface roughness – a roughness height of no more than 100 nm [53, 54].

And the third, most important for our case of determining residual austenite, is to obtain clear identification points during mapping by eliminating residual stresses in the carburized layer by tempering or annealing [53, 54]. If stress is present on the surface and in the surface layer, a diffraction pattern will not form due to a violation of the physical nature of the *EBSD* method, which consists of electrons diffracting on the planes of the crystal lattice and forming unique patterns (*Kikuchi* lines) on the detector. If the crystal lattice is severely distorted, diffraction does not occur and *Kikuchi* lines do not form on the detector. A map is not formed, and instead of identifying the crystal lattice type, solid dark dots are obtained. To relieve residual stresses after heat treatment, high-temperature tempering or annealing is recommended [1, 2]. In our case, this is unacceptable. It is known [1, 2] that residual austenite is already in a state of strong compression after conventional quenching. This occurs because the domains of residual austenite are "encapsulated" between martensite domains and are subjected to compressive stress as a result of the positive volume change during the transformation of residual austenite into martensite.

An important addition is that residual austenite particles smaller than 0.2 μm cannot be indexed by the *EBSD* method [53]. Consequently, the amount of residual austenite depicted in phase maps is underestimated. Furthermore, martensite size is measured according to the different martensite orientations in the inverse pole figure (*IPF*) maps.

Taking into account the above, the data obtained in our study by X-ray diffraction (*XRD*) are reliable given the proven method used, which has an error in measuring residual austenite of up to 0.1% [37, 39, 41, 46, 48, 49]. Table 6 presents data on the residual austenite content in the carburized layer for different paste compositions containing graphite under the following processing conditions: speed of 3 mm/s, laser

Table 6

Amount of retained austenite on the surface of the carburized layer as a function of graphite content in the paste during laser carburizing

Graphite content (%)	Lattice parameter, Å (austenite α_γ)	Lattice parameter, Å (martensite α_α)	Austenite (%) (*XRD*)
10	3.59175	2.87231	5.829724
25	3.58959	2.87278	10.29394
50	3.58777	2.87356	24.983112

power of 1 kW. As a rule, in the martensitic microstructure of high-carbon steels or case-hardened steels with a carbon content of 0.8 wt.%, 30 vol.% or more of austenite can be retained [2]. The carbon content in the surface layer of *0.2% C* steel after laser carburizing from the paste composition (see Table 2) shows that the carbon on the surface can range from 0.8 to 2.2%. The data in Table 6 do not contradict the results obtained with traditional carburizing methods [2].

Our cryogenic treatment of laser-carburized samples yielded positive results (Fig. 13). Traditional hardening is typically performed at ambient temperature, which results in the retention of some residual austenite in the hardened layer. On the other hand, during cryogenic treatment, due to the volume expansion that occurs during the transformation of the austenite phase into the "new martensite" phase, the untransformed residual austenite experiences compressive hydrostatic pressure in all directions, which hinders further transformation [55–59].

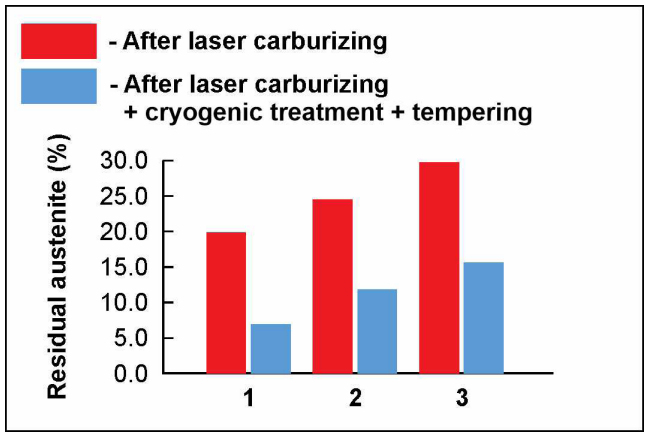

Fig. 13. Results of residual austenite reduction in the carburized surface layer of 0.2% *C* steel after cryogenic treatment for 5 h and subsequent tempering:
1 – 10% graphite coating; 2 – 25% graphite coating; 3 – 50% graphite coating

In our studies, after cryogenic treatment, a "new martensite" phase was formed, which mainly included thin lamellar martensite and lens-shaped martensite, and crystalline defects such as twins were formed in the "new martensite" phase (Figs. 10–12). This is consistent with the results of review papers [55–59], which reported that thermally activated martensite formation can be interpreted as the growth of thin lamellar martensite, which thermally nucleates during cooling into lenticular martensite. Other studies [46–48] have shown that there is a *K–C* orientation relationship between the martensitic and residual austenite phases during the martensite phase transformation. In general, from review works on cryogenic processing of steels, it is believed [55–59] that a strict *K–C* or *H–B* orientation relationship between "new martensite" and residual austenite contributes to the structural stability of the material. The significant increase in this ratio after cryogenic treatment suggests that cryogenic treatment is beneficial in improving the hardness stability of the material (Fig. 12). The formation of a "new martensite" phase increases the dislocation density, and

the source of dislocations can be a thin plate or an isothermal martensite phase [58, 59]. In addition, the high dislocation density around the undissolved carbides increased due to the difference in the thermal expansion coefficients of the matrix structure and the carbides [50]. Some researchers believe that cryogenic treatment can completely eliminate the residual austenite phase [44–47], while others hold the opposite opinion – that it can only reduce the residual austenite content [49, 50]. On the other hand, it is known [1, 2] that the temperature of completion of the martensitic transformation (*Mf*) of high-alloy martensitic steels is lower than ambient temperature. And residual austenite is objectively always present in steel.

From an analysis of review papers [55–59], it can be concluded that cryogenic treatment causes favorable changes in the microstructure of low-carbon carburized and high-carbon steels, leading to increased hardness and improved wear resistance. These improvements are explained by several factors. Most studies attribute the improved properties to a decrease in the content of residual austenite (γ-phase) and an increase in the amount of carbides. Other studies also emphasize the refinement of martensite with a higher dislocation density and fine twinning, the formation of secondary carbides, and the establishment of a more uniform distribution of nanoscale transition precipitates. However, the specific mechanisms determining these improvements and their extent vary depending on the material composition and processing parameters.

At the same time, we note that according to the review paper [58], the cryogenic treatment process schemes play an important role in the cryogenic treatment of steel. There is a discussion about the sequence of heat treatment and its influence on the result of the final treatment. Various sequences have been used [58]. The most frequently used was the "classical" mode with cryogenic treatment after quenching and before tempering, sequence A. However, other sequences such as: (B) sequence without tempering after *CT*; (C) sequence with multiple subsequent quenching and *CT* before tempering; (D) sequence with intermittent cooling or preliminary aging before *CT*; (E) sequence with *CT* after tempering; (F) sequence with preliminary tempering, *CT*, and subsequent tempering; (G) sequence with several *CT*/tempering cycles have a strong influence on the content of residual austenite. The immersion time in a cryogenic environment is the second most important parameter (after the temperature of the cryogenic environment) affecting the microstructure and properties of metals. The cooling rate is the third most important parameter affecting the microstructure and mechanical properties of materials, accounting for 9.34–14% of the changes [58]. The fourth parameter is the exposure time in the cryogenic environment.

In relation to our results, we did not take all these factors into account when conducting the research, which allows us to conduct a comprehensive study of these parameters in the future. At the same time, analyzing the works [56, 57], we can confidently say that holding in a cryogenic environment for 10 hours in our experiments did not provide a positive increase in the effect of reducing residual austenite and an increase in hardness due to the termination of the experiment on our part. However, as the results of work [56] show, a rapid increase in hardness by 1–2 units on the *HRC* scale occurred in the first 2–5 hours, followed by a slow increase in hardness, i.e., in our studies it was necessary to increase the holding time to at least 15–42 hours [56]. Work [56] provides recommendations on the holding time, immersion rate, and temperature of the cryogenic environment for various types of steel, which allows us to further verify these recommendations.

In a number of review articles [55–59] over the past two decades, the authors have discussed the effects of cryogenic treatment on various metals and materials. Despite a significant amount of research confirming the advantages of cryogenic treatment, there remains a need for comprehensive research specifically into surface carburizing methods, where experimental studies are still insufficient. Most of the work in the field of surface hardening using concentrated heat sources [8–22] is aimed at increasing the hardness and wear resistance of steel. One of the main problems of traditional heat treatment of steels by quenching and tempering is the content of residual austenite (γ*R*), which is soft, unstable at low temperatures, and transforms into brittle martensite during operation. The role of residual austenite in the friction process has not yet been fully studied, and what percentage (1, 10, 20, 25%) favorably affects the increase in wear resistance is also a matter of debate. The transformation of austenite into martensite is associated with a volume expansion of approximately 4%, which causes deformation of the components. Thus, to minimize the γ*R* content in steels, either treatment at sub-zero temperatures or repeated tempering at relatively high temperatures and/

or for longer periods are used. The advantages of cryogenic treatment for increasing the wear resistance of steels have been noted by researchers [46–48]. However, the mechanisms responsible for the increase in wear resistance during cryogenic treatment have not yet been established. Some researchers [46–48, 56, 57] argue that the increase in wear resistance occurs solely due to the transformation of γR into martensite. However, this phenomenon is a common feature of both cold treatment (down to –80 °C) and cryogenic treatment (–196 °C), and therefore the significant increase in wear resistance of steels during cryogenic treatment compared with cold treatment cannot be explained solely by the minimization of γR.

Although the mechanism underlying the improved wear resistance during cryogenic treatment has not yet been fully elucidated, the presented wear data on cryogenically treated steels also do not provide any indication for quantifying the degree of improvement. Therefore, it is difficult to summarize the existing results to obtain a unified picture. In our future research, we will continue this work, specifically by conducting wear tests on specimens with varying residual austenite contents in the surface layer after laser carburizing.

Conclusions

1. It has been established that during laser surface carburizing at a scanning speed of 3 mm/s and a laser power of 1 kW, using a graphite powder mixture with a concentration of 10 to 50%, residual austenite is formed in the carburized layer within the range of 5.8–24.9%.

2. Diffraction peaks for γ, namely (200), (220), and (311), as well as peaks for α (200) and (211), were analyzed. Peaks corresponding to hardened martensite and residual austenite were detected. The maximum amount of residual austenite is observed at depths ranging from 60 to 280 μm, with values varying between 11 and 21%.

3. Cryogenic treatment of samples after laser carburizing with an exposure time of 2–5 hours, followed by subsequent tempering, allows a 1.5- to 2-fold reduction in the amount of residual austenite in the carburized layer. Cryogenic treatment for 10 hours did not result in any additional reduction of residual austenite.

4. Cryogenic treatment of samples after laser carburizing with an exposure time of 2–5 hours, followed by subsequent tempering, significantly increases hardness. Macrohardness on the *HRC* scale increases by 1–2 units, while microhardness on the *Vickers* scale increases by 100–180 units.

References

1. Filippov M.A., Kositsyna I.I., Gervas'ev M.A. *Uprochnenie i zashchita poverkhnosti metallov* [Hardening and protection of metal surfaces]. Ekaterinburg, Ural Branch of the Russian Academy of Sciences Publ., 2012. 234 p.

2. Lakhtin Yu.M., Arzamasov B.N. *Khimiko-termicheskaya obrabotka metallov* [Chemical-thermal treatment of metals]. Moscow, Metallurgiya Publ., 1985. 256 p.

3. Madu M.J., Adedipe O., Lawal S.A., Abdulrahman A.S. The influence of carburization parameters on the mechanical behavior of mild steel: a review. *Journal of Engineering and Applied Science*, 2025, vol. 72 (1), p. 193. DOI: 10.1186/s44147-025-00776-9.

4. Jumadin M.H., Abdullah B., Ismail M.H., Alias S.K., Ahmad S. Effect of soaking time on paste carburizing of carburized low carbon steel. *Key Engineering Materials*, 2017, vol. 740, pp. 93–99. DOI: 10.4028/www.scientific.net/KEM.740.93.

5. Qin S., Zhang C., Zhang B., Ma H., Zhao M. Effect of carburizing process on high cycle fatigue behavior of 18CrNiMo7-6 steel. *Journal of Materials Research and Technology*, 2022, vol. 16, pp. 1136–1149. DOI: 10.1016/j.jmrt.2021.12.074.

6. Abdenour S., Linda A., Oualid C., Ali B., Salah L.M., Hamid D., Francisco C. Influence of the carburization time on the structural and mechanical properties of XC20 steel. *Materials Research Express*, 2021, vol. 8 (8), p. 085604. DOI: 10.1088/2053-1591/ac1ece.

7. Zhou Y.-L., Xia F., Xie A.-J., Peng H.-P., Wang J.-H., Li Z.-W. A review – Effect of accelerating methods on gas nitriding: accelerating mechanism, nitriding behavior, and techno-economic analysis. *Coatings*, 2023, vol. 13 (11), p. 1846. DOI: 10.3390/coatings13111846.

8. Song H., Tao F. Laser-assisted coating techniques and surface modifications. *Coatings*, 2026, vol. 16 (4), p. 430. DOI: 10.3390/coatings16040430.

9. Shin W.-S., Yoo H.J., Kim J.H., Choi J., Chun E.-J., Park C., Kim Y.-J. Effect of laser heat-treatment and laser nitriding on the microstructural evolutions and wear behaviors of AISI P21 mold steel. *Metals*, 2020, vol. 10 (11), p. 1487. DOI: 10.3390/met10111487.

10. Brover G.I., Brover A.V., Dyachenko L.D. Struktura i svoistva instrumental'nykh stalei posle obrabotki razlichnymi istochnikami kontsentrirovannykh potokov energii [Structure and Properties of Tool Steels after Treatment with Various Sources of Concentrated Energy Flows]. *Uprochnyayushchie tekhnologii i pokrytiya = Strengthening Technologies and Coatings*, 2005, no. 12, pp. 27–31.

11. Chudina O.V. *Kombinirovannye metody poverkhnostnogo uprochneniya stalei s primeneniem lazernogo nagreva: teoriya i tekhnologiya* [Combined methods of surface hardening of steels using laser heating: theory and technology]. Moscow, MADI Publ., 2003. 248 p.

12. Grigoryants A.G., Shiganov I.N., Misyurov A.I. *Tekhnologicheskie protsessy lazernoi obrabotki* [Technological processes of laser processing]. Moscow, Bauman MSTU Publ., 2006. 664 p.

13. Losinskaya A.A., Lozhkina E.A., Bardin A.I. Structure and properties of steel case-hardened by non-vacuum electron-beam cladding of carbon fibers. *IOP Conference Series: Materials Science and Engineering*б 2017, vol. 286, p. 012036. DOI: 10.1088/1757-899X/286/1/012036.

14. Bataev I.A., Golkovskii M.G., Bataev A.A., Losinskaya A.A., Dostovalov R.A., Popelyukh A.I., Drobyaz E.A. Surface hardening of steels with carbon by non-vacuum electron-beam processing. *Surface and Coatings Technology*, 2014, vol. 242, pp. 164–169. DOI: 10.1016/j.surfcoat.2014.01.038.

15. Bataev I.A., Golkovskii M.G., Losinskaya A.A., Bataev A.A., Popelyukh A.I., Hassel T., Golovin D.D. Non-vacuum electron-beam carburizing and surface hardening of mild steel. *Applied Surface Science*, 2014, vol. 322, pp. 6–14. DOI: 10.1016/j.apsusc.2014.09.137.

16. Skorynina P.A., Makarov A.V., Menshakov A.I., Osintseva A.L. Vliyanie nizkotemperaturnoi tsementatsii v plazme elektronnogo puchka na uprochnenie i sherokhovatost' poverkhnosti metastabil'noi austenitnoi stali [Effect of low-temperature carburizing in electron beam plasma on the hardening and surface roughness of metastable austenitic steel]. *Obrabotka metallov (tekhnologiya, oborudovanie, instrumenty) = Metal Working and Material Science*, 2019, vol. 21 (2), pp. 97–109. DOI: 10.17212/1994-6309-2019-21.2-97-109.

17. Losinskaya A.A., Drobyaz E.A., Bataev V.A., Plotnikova N.V., Golkovsky M.G. Struktura i svoistva poverkhnostnykh sloev nizkouglerodistoi stali, poluchennykh metodom naplavki uglerodsoderzhashchikh poroshkovykh smesei i posleduyushchei zakalki [Structure and properties of surface layers of low-carbon steel obtained by surfacing carbon-containing powder mixtures and subsequent hardening]. *Obrabotka metallov (tekhnologiya, oborudovanie, instrumenty) = Metal Working and Material Science*, 2013, no. 4 (61), pp. 5–11.

18. Savrai R.A., Skorynina P.A., Makarov A.V., Men'shakov A.I., Gaviko V.S. Vliyanie friktsionnoi obrabotki i nizkotemperaturnoi plazmennoi tsementatsii na strukturu i fazovyi sostav metastabil'noi austenitnoi stali [The influence of frictional treatment and low-temperature plasma carburizing on the structure and phase composition of metastable austenitic steel]. *Fizika metallov i metallovedenie = Physics of Metals and Metallography*, 2023, vol. 124, no. 5, pp. 409–416. DOI: 10.31857/S0015323023600442.

19. Savrai R.A., Skorynina P.A., Makarov A.V., Osinceva A.L. Structure and surface properties of metastable austenitic steel subjected to liquid carburizing at a reduced temperature. *Physics of Metals and Metallography*, 2020, vol. 121 (1), pp. 65–71. DOI: 10.1134/S0031918X20010135.

20. Savrai R.A., Skorynina P.A., Makarov A.V., Osinceva A.L. Effect of liquid carburizing at lowered temperature on the micromechanical characteristics of metastable austenitic steel. *Physics of Metals and Metallography*, 2020, vol. 121 (10), pp. 1015–1020. DOI: 10.1134/S0031918X20100105.

21. Karlina Y.I., Balanovskiy A.E., Kurdyumov G.E., Gladkikh V.A., Konyukhov V.Y., Oparina T.A., Kononenko R.V., Kondratiev V.V. Visualization of the reverse side of cathode and anode spots in a welding arc. *Applied Sciences*, 2026, vol. 16, p. 3385. DOI: 10.3390/app16073385.

22. Balanovsky A.E., Vu Van Huy. Nasyshchenie poverkhnosti metalla uglerodom pri plazmennoi poverkhnostnoi obrabotke [Saturation of the metal surface with carbon during plasma surface treatment]. *Uprochnyayushchie tekhnologii i pokrytiya = Strengthening Technologies and Coatings*, 2017, vol. 13, no. 9 (153), pp. 82–91.

23. Vu Van Huy, Balanovsky A.E. Issledovanie iznosostoikosti poverkhnosti stali posle plazmennoi tsementatsii s ispol'zovaniem uglerodosoderzhashchei pasty [Study of wear resistance of steel surface after plasma carburizing using carbon-containing paste]. *Vestnik Irkutskogo gosudarstvennogo tekhnicheskogo universiteta = Bulletin of Irkutsk State Technical University*, 2017, vol. 21, no. 4, pp. 10–21.

24. Vu Van Huy, Balanovsky A.E. Fizicheskie osnovy tekhnologii plazmennoi poverkhnostnoi tsementatsii detalei na primere vtulki shpintona passazhirskogo vagona [Physical principles of plasma surface carburizing of parts as exemplified by an antirattle bushing of a passenger coach]. *Vestnik Irkutskogo gosudarstvennogo tekhnicheskogo universiteta = Bulletin of Irkutsk State Technical University*, 2017, vol. 21, no. 3, pp. 10–22.

25. Balanovskii A., Vu Van Huy. Plasma surface carburizing with graphite paste. *Letters on Materials,* 2017, vol. 7 (2), pp. 175–179. DOI: 10.22226/2410-3535-2017-2-175-179.

26. Balanovskii A.E., Grechneva M.V., Vu Van Huy, Zhuravlev D.A. New plasma carburizing method. *IOP Conference Series: Earth and Environmental Science*, 2017, vol. 87, p. 092003. DOI: 10.1088/1755-1315/87/9/092003.

27. Vu V.H., Balanovskiy A.E., Doan V.T., Nguyen V.T. Surface saturation with carbon using plasma arc and graphite coating. *Tribology in Industry*, 2021, vol. 43 (2), pp. 211–221. DOI: 10.24874/ti.951.08.20.12.

28. Balanovskiy A.E. Digital visualisation of the process of heating and melting of metal in arc discharge with a non-consumable electrode. *Welding International*, 2017, vol. 31 (6), pp. 467–476. DOI: 10.1080/09507116.2016.1268765.

29. Höche D., Kaspar J., Schaaf P. 2 – Laser nitriding and carburization of materials. *Laser surface engineering: processes and applications*. Ed. by J. Lawrence and D.G. Waugh. *Woodhead Publishing Series in Electronic and Optical Materials*, no. 65. Elsevier, 2015, pp. 33–58. DOI: 10.1016/B978-1-78242-074-3.00002-7.

30. Katsamas A.I., Haidemenopoulos G.N. Laser-beam carburizing of low-alloy steels. *Surface and Coatings Technology*, 2001, vol. 139 (2–3), pp. 183–191. DOI: 10.1016/S0257-8972(00)01061-6.

31. Maharjan N., Zhou W., Wu N. Direct laser hardening of AISI 1020 steel under controlled gas atmosphere. *Surface and Coatings Technology*, 2020, vol. 385, p. 125399. DOI: 10.1016/j.surfcoat.2020.125399.

32. Zhang J., Yu M., Li Z., Liu Y., Zhang Q., Jiang R., Sun S. The effect of laser energy density on the microstructure, residual stress and phase composition of H13 steel treated by laser surface melting. *Journal of Alloys and Compounds*, 2021, vol. 856, p. 158168. DOI: 10.1016/j.jallcom.2020.158168.

33. Kluczyński J., Jasik K., Łuszczek J., Pokropek J. laser surface hardening of carburized steels: a review of process parameters and application in gear manufacturing. *Materials*, 2025, vol. 18 (15), p. 3623. DOI: 10.3390/ma18153623.

34. Pozdnyakov E.P., Stepankin I.N. Vliyanie dlitel'nosti tsementatsii na strukturu i svoistva konstruktsionnykh sredneuglerodistykh stalei 40Kh, 35KhGSA i 42CrMoS4 [Influence of cementation duration on the structure and properties of structural middle carbon steel 40Cr4, 35CrMnSi4 and 42CrMoS4]. *Lit'e i metallurgiya = Foundry Production and Metallurgy*, 2024, no. 1, pp. 69–77. DOI: 10.21122/1683-6065-2024-1-69-77.

35. Karlina Yu.I., Konyukhov V.Yu., Oparina T.A. Issledovanie protsessa poverkhnostnogo obezuglerozhivaniya stali 20 posle tsementatsii i termicheskoi obrabotki [Investigation of the process of surface decarburization of steel 20 after cementation and heat treatment]. *Obrabotka metallov (tekhnologiya, oborudovanie, instrumenty) = Metal Working and Material Science*, 2025, vol. 27, no. 3, pp. 122–136. DOI: 10.17212/1994-6309-2025-27.3-122-136.

36. Wong A. Modelling the stability and transformation kinetics of retained austenite in steels. *Materials Science and Technology*, 2022, vol. 38 (11), pp. 676–688. DOI: 10.1080/02670836.2022.2063539.

37. Xiong X.C., Chen B., Huang M.X., Wang J.F., Wang L. The effect of morphology on the stability of retained austenite in a quenched and partitioned steel. *Scripta Materialia*, 2013, vol. 68 (5), pp. 321–324. DOI: 10.1016/j.scriptamat.2012.11.003.

38. Sidoroff C., Perez M., Dierickx P., Girodin D. Advantages and shortcomings of retained austenite in bearing steels: a review. *Bearing Steel Technologies: 10th Volume, Advances in Steel Technologies for Rolling Bearings*, ASTM International, 2014, pp. 1–37. DOI: 10.1520/STP158020140081.

39. Shen Y., Moghadam S.M., Sadeghi F., Paulson K., Trice R.W. Effect of retained austenite –Compressive residual stresses on rolling contact fatigue life of carburized AISI 8620 steel. *International Journal of Fatigue*, 2015, vol. 75, pp. 135–144. DOI: 10.1016/j.ijfatigue.2015.02.017.

40. Evans M.H. An updated review: white etching cracks (WECs) and axial cracks in wind turbine gearbox bearings. *Materials Science and Technology*, 2016, vol. 32 (11), pp. 1133–1169. DOI: 10.1080/02670836.2015.1133022.

41. Kumar S., Singh S.B. Quantification of retained austenite in low-carbon steels. *Metallurgical and Materials Transactions A*, 2023, vol. 54 (11), pp. 4283–4294. DOI: 10.1007/s11661-023-07162-1.

42. Ionescu L.G., Pantawane M.V., Tănase C., Sichim R.V., Dascălu C.A., Ghiban B. Evaluation of retained austenite in carburized bearing steel using magneto-inductive method. *Crystals*, 2023, vol. 13 (8), p. 1173. DOI: 10.3390/cryst13081173.

43. Zhu Z., Liang Y. Prediction of residual stress of carburized steel based on machine learning. *Applied Sciences*, 2020, vol. 10 (21), p. 7759. DOI: 10.3390/app10217759.

44. Wei S., Wang G., Zhao X., Zhang X., Rong Y. Experimental study on vacuum carburizing process for low-carbon alloy steel. *Journal of Materials Engineering and Performance*, 2014, vol. 23 (2), pp. 545–550. DOI: 10.1007/s11665-013-0762-1.

45. Muñoz-Rodenas J., García-Sevilla F., Coello-Sobrino J., Martínez-Martínez A., Miguel-Eguía V. Effectiveness of machine-learning and deep-learning strategies for the classification of heat treatments applied to low-carbon steels based on microstructural analysis. *Applied Sciences*, 2023, vol. 13, p. 3479. DOI: 10.3390/app13063479.

46. Jovičević-Klug P., Podgornik B. Review on the effect of deep cryogenic treatment of metallic materials in automotive applications. *Metals*, 2020, vol. 10 (4), p. 434. DOI: 10.3390/met10040434.

47. Yan Y., Liu K., Luo Z., Wang M., Wang X. Effect of cryogenic treatment on microstructure, mechanical properties and distortion of carburized gear steels. *Metals*, 2021, vol. 11, p. 1940. DOI: 10.3390/met11121940.

48. Ďurica J., Ptačinová J., Dománková M., Čaplovič L., Čaplovičová M., Hrušovská L., Malovcová V., Jurči P. Changes in microstructure of ledeburitic tool steel due to vacuum austenitizing and quenching, sub-zero treatments at – 140°C and tempering. *Vacuum*, 2019, vol. 170, p. 108977. DOI: 10.1016/j.vacuum.2019.10897.

49. ASTM E975-13. *Standard Practice for X-Ray Determination of Retained Austenite in Steel with Near Random Crystallographic Orientation*. West Conshohocken, PA, USA, ASTM International, 2013.

50. Zhao J., Zhao X., Zhao X., Dong C., Kang S. Effects of nucleation site and morphology of carbide-free bainite on microstructures and properties of bainite/martensite multi-phase steels. *Materials Science and Engineering: A*, 2019, vol. 744, pp. 86–93. DOI: 10.1016/j.msea.2018.11.060.

51. Wingens T. Techniques for determining retained austenite. *AM&P Technical Articles*, 2022, vol. 180, pp. 60–64. DOI: 10.31399/asm.amp.2022-05.p060.

52. Koistinen D., Marburger R. A general equation prescribing the extent of the austenite-martensite transformation in pure iron-carbon alloys and plain carbon steels. *Acta Metallurgica*, 1959, vol. 7, pp. 59–60. DOI: 10.1016/0001-6160(59)90170-1.

53. Varyukhin V.N., Pashinskaya E.G., Zavdoveev A.V., Burkhovetskii V.V. *Vozmozhnosti metoda difraktsii obratno-rasseyannykh elektronov dlya analiza struktury deformirovannykh materialov* [Possibilities of the Electron Backscatter Diffraction Method for Analysis of the Structure of Deformed Materials]. Kyiv, Naukova Dumka Publ., 2014. 102 p. DOI: 10.13140/2.1.5016.6720.

54. Doddapaneni S., Kumar S., Sharma S., Shankar G., Shettar M., Kumar N., Aroor G., Ahmad S.M. Advancements in EBSD techniques: a comprehensive review on characterization of composites and metals, sample preparation, and operational parameters. *Journal of Composites Science,* 2025, vol. 9 (3), p. 132. DOI: 10.3390/jcs9030132.

55. Kalsi N.S., Sehgal R., Sharma V.S. Cryogenic treatment of tool materials: a review. *Materials and Manufacturing Processes*, 2010, vol. 25 (10), pp. 1077–1100. DOI: 10.1080/10426911003720862.

56. Singla A.K., Singh J., Sharma V.S. Processing of materials at cryogenic temperature and its implications in manufacturing: a review. *Materials and Manufacturing Processes*, 2018, vol. 33 (15), pp. 1603–1640. DOI: 10.1080/10426914.2018.1424908.

57. Reitz W., Pendray J. Cryoprocessing of materials: a review of current status. *Materials and Manufacturing Process*es, 2001, vol. 16 (6), pp. 829–840. DOI: 10.1081/AMP-100108702.

58. Jurči P., Dlouhý I. Cryogenic treatment of martensitic steels: microstructural fundamentals and implications for mechanical properties and wear and corrosion performance. *Materials*, 2024, vol. 17, p. 548. DOI: 10.3390/ma1703054.

59. Senthilkumar D., Rajendran I. A research review on deep cryogenic treatment of steels. *International Journal of Materials and Structural Integrity*, 2014, vol. 8, pp. 169–184. DOI: 10.1504/IJMSI.2014.064784.

Conflicts of Interest

The authors declare no conflict of interest.